2024

Searching for Black Holes in the Galactic Center

Caden Zaccardi
University of Central Florida, ca630054@ucf.edu

SEARCHING FOR BLACK HOLES IN THE GALACTIC CENTER

by

CADEN ZACCARDI
B.S. Florida Atlantic University, 2021

A thesis submitted in partial fulfilment of the requirements
for the Honors Undergraduate Thesis program in Physics
in the College of Sciences
and in the Burnett Honors College
at the University of Central Florida
Orlando, Florida

Spring Term
2024

Thesis Chair: Stephen Eikenberry

ABSTRACT

Due to the high extinction along the plane of the Milky Way towards the Galactic Center (GC), it is useful to look at objects that are bright in the near-infrared (near-IR) to obtain data with Earth-based instruments. To identify X-ray Binary (XRB) counterparts towards the GC, we used near-IR spectra from the Large Binocular Telescope (LBT). After reducing the LUCI/LBT spectra with the superFATBOY (sFB) pipeline, we compared our near-IR spectra to previously matched IR and X-ray sources in the GC [DeWitt, 2011]. Particularly, we looked for H and He emission lines, which indicate signs of a hard radiation field present with typically red giant or red supergiant stars in the GC. This illustrates a likely physical association between the X-ray source and its IR counterpart.

ACKNOWLEDGMENTS

Special thanks to Craig Warner for guiding me through the many errors I had with superFATBOY. This data reduction could not have been done without Craig or the expertise of my HUT advisor, Dr. Eikenberry.

Thank you to Dr. Eikenberry for agreeing to do the HUT program with me, challenging me, and furthering my growth as an astrophysicist. It is with this honors thesis and my previous research project with Dr. Vicki Sarajedini that bring me to continue my studies in a PhD program in the future.

TABLE OF CONTENTS

LIST OF FIGURES

LIST OF TABLES

CHAPTER 1: INTRODUCTION

Within the inner region of our Milky Way, expanding about sixty light years from the galactic nucleus, lies thousands of X-ray sources. Neutron stars, black holes (BHs), hot gas, binaries with white dwarf stars, and stellar atmospheres are several of these X-ray point sources. Within the innermost region, expanding about twelve light years, contains hundreds of these x-ray point sources [Hailey et al., 2018]. The environment within this inner region towards the barycenter of our galaxy, the Galactic Center (GC), differs from the rest of our galaxy and have posed X-ray binary (XRB) candidates to hold different characteristics compared to XRBs outside of this region [Gottlieb, 2021]. In my thesis, I will be focusing on finding new XRBs and studying the characteristics of these candidates such as seeing if accretion is present and identifying the spectral class of their donor star. Along this, a further revision will be made where I will be studying the characteristics of known XRB XID 6592, potential XRB XID 13 (Both discovered by DeWitt, 2011), and Star 5 (Discovered by Garner, 2018). Where Star 5 has shown to be an XRB with a potential BH as it's compact object (BH-XRB). This revision will be made after our Gemini South observations in May, June, and July of 2024.

X-ray Binaries

An X-ray binary is a type of binary system that consists of a compact object and companion donor star. These compact objects can be a BH or neutron star. These systems

produce X-rays due to the star's matter accreting onto the compact object, which ionizes the star's matter. There is a similar binary system with a white dwarf (WD) as their compact object, called a cataclysmic variable (CV), that also has a star and accretion on the compact object.

Of these compact objects, WDs can be easy to locate due to it's high relative brightness, this is not the case with an isolated BH or NS. NSs are very dim being only $\sim$ 10km in diameter, and BHs are so dense that not even light can escape their gravitational well. Without accretion, you cannot detect a BH. Although, there are ways to observe and locate such BHs, which is by finding an XRB. The type of compact object in these XRBs can be identified by observing the gravitational effects the compact object has on it's donor star by measuring the radial velocity of the star. If the radial velocity is measured over time, the orbital period can then be deduced, and with the orbital period and peak radial velocity of the donor star, we can determine the binary mass function of the system. With this, we can classify what kind of compact object is present, whether it is a BH or NS [Gottlieb, 2021]. There are also strategies to identify the spectral class and class sub-type of the donor star which involves looking at the stellar absorption lines and equivalent widths of those absorption lines in the XRB's spectrum [Gottlieb, 2021].

There are sub-classes of XRBs that classifies the mass of the donor star in the system. Two of which are a low-mass X-ray binary (LMXB) and a high-mass X-ray binary (HMXB).

A LMXB contains a compact object and a low mass donor star with a mass $1M_{\odot}$ and a lifetime of $\sim 10^{10}$years [Neumann et al., 2023]. In a LMXB, the donor star overfills

its Roche lobe, which is a defined region around a star in a binary system where orbiting material is gravitationally bound to the star. Due to the overflow, it causes orbiting material to spill out of this region that is then accreted onto the compact object. These donor stars are usually late-type stars. However, A-type stars, F-G-type subgiants, or even WDs can be donors in LMXBs [Avakyan et al., 2023]. LMXBs are mostly discovered from their variable luminosities due to the changes in accretion rate and can reach a max luminosity of 10^{37} to 10^{39} ergs s^{-1} for weeks to months, then go into quiescence of luminosities of 10^{32} to 10^{33} ergs s^{-1} up to tens of years [Tauris and van den Heuvel, 2006].

These LMXBs can be further defined into sub-classes. The most common is a lower luminosity dwarf as the donor and a NS as the compact object with the same properties above [Gottlieb, 2021]. The more rare sub-class is the symbiotic X-ray binary (SXB). SXBs host a red giant as its donor and a NS as its compact object (most commonly), which accretes from the donor's stellar winds. The behavior of SXBs greatly resemble the behavior of HMXBs, which will be covered later. SXBs have the longest orbital periods of LMXBs from several tens to a thousand days and have long pulse periods from hundred of seconds to hours. They have strong X-ray variability of a factor of ~ 10 to 20 times that of an HMXB. This suggests the NS compact object is highly magnetized of at least 10^{12} G [Bozzo et al., 2022].

A HMXB contains a compact object and a high-mass donor star with a mass $5M_{\odot}$, with their lifetime being shorter than a LMXB at $\sim 2 \times 10^{7}$years [Neumann et al., 2023]. HMXBs can be defined further into several sub-classes. One of which, making up most of the HMXB population would be Be X-ray binaries (BeXBs). The donor star in BeXBs

are typically early-type B or late-type O stars with decretion disks around their equator, which is material distributed in the shape of a disk that is centered around the body. Due to the high rotational velocity such a decretion disk is formed [Balona and Ozuyar, 2020]. Currently, the compact object in BeXBs are almost always NS and only a few have BHs as their compact object. BeXBs are most often found when they are experiencing outbursts from the compact object passing through the decretion disk causing enhanced accretion. There is Type I and Type II outbursts, with Type I being periodic with peak luminosity below 10^{37} erg s^{-1} and Type II being less frequent with a peak velocity up to 10^{39} erg s^{-1} [Doroshenko et al., 2020].

The other two sub-classes are Supergiant X-ray binaries (SGXBs) and Supergiant Fast X-ray transients (SFXTs). The compact object, most typically NS, in SGXBs accrete from the stellar winds from the supergiant donor star with mass loss rates of up to $\sim 10^{-6}$ to 10^{-5} y^{-1} [Kudritzki and Puls, 2000]. SGXBs have short orbital periods and have a similar range of X-ray luminosity as BeXBs of 10^{36} to 10^{37} ergs s^{-1} [Gottlieb, 2021]. In rare cases, accretion can happen due to Roche lobe overflow, which produces higher X-ray luminosities than those systems that accrete from stellar winds [Fortin et al., 2023]. SFXTs are a sub-class of SGXBs that do not accrete a majority of the time, but have bright flares that happen on timescales of minutes to days with peak fluxes similar to SGXBs [Neumann et al., 2023].

Systems in which a WD acts as the compact object and accretes its donor star are not considered XRBs despite the fact that they emit X-rays [Avakyan et al., 2023]. These systems are referred to as CVs. CVs have a low-mass donor star and the WD accretes

via Roche lobe overflow similarly to LMXBs. They have overall lower X-ray luminosities than most XRBs ranging from $10^{29.5}$ to 10^{32} ergs s^{-1} and are not commonly detected in X-rays [Gottlieb, 2021].

There is a sub-class of CVs that produce hard X-rays called intermediate polars (IPs). IPs have more extreme magnetic fields than normal CVs ranging from 10^6 to 10^8 G [Perez et al., 2015], which happen due to increased temperature and density of material that is funnelled into the poles via the magnetic field.

The Galactic Center

The GC is defined by a $2^\circ \times 0.8^\circ$ center region which is composed of $\sim 1\%$ of the stellar mass of the Milky Way [Launhardt et al., 2002]. The environment within the GC differs from the rest of our galaxy due to it's close proximity to the Milky Way's supermassive black hole, Sagittarius A* (Sgr A*), which has a mass of $(4.297 \pm 0.012) \times 10^6 M_\odot$ [GRAVITY Collaboration et al., 2023]. This region is more hot, turbulent, and highly magnetized [Mauerhan et al., 2010]. The GC was found to have over 10,000 X-ray sources, primarily by the Chandra X-ray Observatory, and a majority of these points were located within the GC or beyond it [Muno et al., 2009]. Due to the large amount of interstellar extinction, the excess of dust obscures our view to look at these sources that have energies below 1.5 keV, and therefore, our understanding of these X-ray sources are generally unknown. Chandra observations of the GC have shown CVs as well as WDs, BHs, and NS [Morihana et al., 2022].

Within the central parsec towards the GC, there lies $\sim 1-4\times10^4$ BHs and it is predicted that $\sim 60-200$ exist as BH-XRBs [Generozov et al., 2018]. It was found that the number of NS-XRBs per stellar mass in the GC is three orders of magnitude greater than in the field, and is comparable to the number found in globular clusters. The number of BH-XRBs are also three orders of magnitude greater than in the field. However, it is an order of magnitude greater than in any existing globular, which indicates that GC BH-XRBs are not brought in by in-fall from globular clusters. It is also unlikely they would be able to survive to the present day, since the lifetime of BH-XRBs are no higher than a few $\times10^9$ yr. This suggests that the unusual environment of the GC dynamically assembles BH-XRBs, similarly to the high production of NS-XRBs in globular clusters. Due to the high density of compact objects and stellar objects in the GC, it is inevitable that there will be a high rate of tidal captures, which could explain the amount of BH-XRBs and NS-XRBs [Generozov et al., 2018].

Hailey et al. [2018] found twelve soft X-ray sources, identified as quiescent low-mass X-ray binaries (qLMXBs), within one parsec outwards of Sgr A* that were found to be consistent with being BH-XRBs. In another paper, Zhu et al. [2018] identified 1300 magnetic and non-magnetic CVs and claimed that qLMXBs are a minority within the GC. In a recent paper, Neumann et al. [2023] compiled a sample[1] of 123 known HMXBs and 46 HMXB candidates from the SIMBAD and VizieR archives hosted by the Centre de Données astronomiques de Stras-bourg databases. I found that ten of these were within the $2^\circ\times0.8^\circ$ region of the GC, where one of them, 1E 1740.7-2942, was classified as a microquasar. Eight of these were transient X-ray sources, with 4 of these having a supergiant

[1] A web-version is publicly accessible at `http://astro.uni-tuebingen.de/~xrbcat/`.

donor star.

It is relevant to keep in mind that all of these findings were based on the understanding of XRBs as they are outside of the GC, and as previously mentioned, the environment of the GC is unusual.

Statement of Problem

Located in the Scutum constellation resides Scutum X-1, the only XRB known to have a red supergiant (RSG) as its donor star outside of the GC. Gottlieb et al. [2020] found that the XRB XID 6592 in the GC closely resembled Scutum X-1's X-ray luminosity, absolute magnitude, and variability in the infrared, which indicated it to also host a RSG donor star. It was also confirmed that 6 XRBs previously discovered by [Garner, 2018] in the GC all had at least a red giant (RG) donor star [Gottlieb, 2021]. XRBs with RG or RSG donor stars have not been seen elsewhere in these amounts as they are in the GC.

CHAPTER 2: LITERATURE REVIEW

XID 13 is a potential XRB located towards the GC at RA = 266.259360" and Dec = 28.963730". Its spectrum in the near-infrared by Folded port InfraRed Echellette (FIRE) shows a Brγ emission line (Figure 2.1), which is characteristic of an accretion disk. However, the spectral type of its donor star was unable to be determined in the preliminary data reduction [DeWitt, 2011].

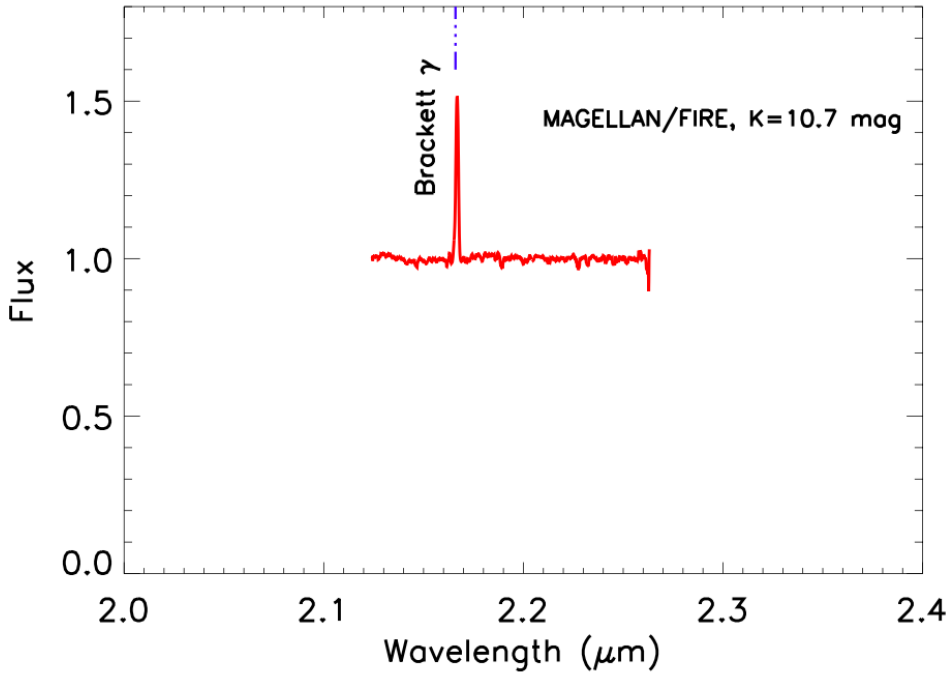

Figure 2.1: Preliminary NIR spectrum for the counterpart to XID 13, observed with FIRE [DeWitt, 2011].

XID 6592 is an XRB located towards the GC at RA $= 17^h45^m28.79^s$ and Dec $= -29°09'42.8''$ ($l = 359.791396°$, $b = -0.091492°$). Its spectrum in the near-infrared by Ohio State InfraRed Imager/Spectrometer (OSIRIS) has shown a Brγ emission line which indicates accretion (Figure 2.2). XID 6592 has a bright X-ray luminosity at $\sim 10^{33}$ ergs s^{-1} [Gottlieb, 2021]. Its spectrum has also shown broad CO absorption bands which are characteristic of late type stars. Gottlieb [2021], determined that XID 6592 has a fast variability of ~ 0.5 mag in a few hours in the IR in the WISE 1 band and has shown variability in the X-rays in both Chandra and the X-ray Multi-Mirror Mission-Newton (XMM). It is hypothesized that XID 6592 is a SFXT with a RSG as a companion star, which would be the first SFXT known with a RSG donor star.

More spectra of XID 6592 in the Ks band was obtained with FLAMINGOS-2 and Espectrógrafo Multiobjeto Infra-Rojo (EMIR), and no significant Brγ emission nor variability was found, which could imply no significant accretion was present during the time of observation. There was also no variability in radial velocities during tens of days. However, there was significant variability in the CO bands after combining the FLAMINGOS-2 and EMIR data, and heavy elements like Scandium were detected [Gottlieb, 2021]. It was confirmed in Gottlieb et al. [2020] that XID 6592 has a RSG donor star as mentioned earlier.

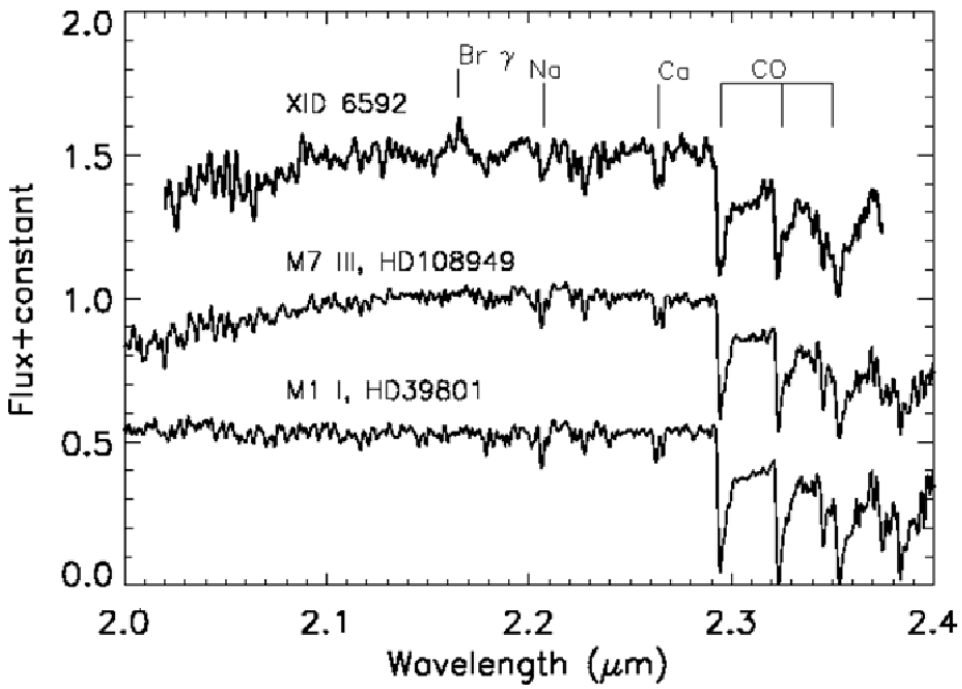

Figure 2.2: OSIRIS K-band spectrum of the counterpart to XID 6592. Also shown is the best-fit M7 III spectrum and the best-fit M12 I spectrum. The M I templates all have deeper CO bands than the counterpart to XID 6592, and therefore we adopt the best-fit M III subtype, M7 III, for this star [DeWitt et al., 2013].

Garner [2018], identified 35 variable and transient infrared sources in the GC using difference imaging on Canarias InfraRed Camera Experiment (CIRCE) data with Zernike polynomials to create a model point spread function of stars. These sources were then cross referenced with Chandra X-ray source catalogs [Muno et al., 2009], where 6 of the variable IR sources matched with X-ray sources. These 6 sources are likely to be XRBs

due to their X-ray and IR luminosities. Their RA and Dec is shown in the table below [Garner, 2018].

Garner GC Sources							
ID	RA	Dec	RA	Dec	RA_{X-ray}	Dec_{X-ray}	M_{Ks}
2	266.42565	-28.943171	17:45:42.16	-28:56:35.42	17:45:42.0	-28:56:36	10.2
5	266.42572	-28.957432	17:45:42.17	-28:57:26.76	17:45:42.1	-28:57:25	11.5
6	266.43009	-28963417	17:45:43.22	-28:57:48.30	17:45:43.3	-28:57:49	9.25
19	266.39131	-29.000519	17:45:33.91	-29:00:01.87	17:45:33.8	-29:00:03	10.4
20	266.39087	-29.012552	17:45:33.81	-29:00:45.19	17:45:33.9	-29:00:43	11.1
26	266.41038	-29.034367	17:45:38.49	-29:02:03.72	17:45:38.4	-29:02:02	8.52

Table 2.1: CIRCE IR RA and Dec and Chandra X-ray RA and Dec of Star 2, Star 5, Star 6, Star 19, Star 20, and Star 26 [Garner, 2018].

Gottlieb [2021], did further spectroscopy on these 6 XRBs and found that all 6 of the companion stars are at least RGs by looking at their equivalent widths and CO indices. Star 5 had a presence of a Brγ line in their first round of observations, and no longer had a Brγ line in the second, indicating no accretion during the second observation. For the rest of the 5 stars, there was no Brγ line detected for either observations. No evidence of variability in their equivalent widths of the CO bands was found in the second observation, when previously they were varying in the first observations done with EMIR. Star 5's compact object was found to be a potential stellar-mass BH, and Star 26 was found to have an inordinately high peak radial velocity for the GC and is likely to be a hyper-velocity star. Based on the CO index of Star 5, it is uncertain whether Star 5's donor star is a RG or

RSG. Below are the lower limits on the mass of the compact object and donor star of Star 5 using different eccentricities [Gottlieb, 2021]. If Star 5 is to be a confirmed BH-XRB, than it would be the first stellar-mass BH in the GC to have a recorded mass measurement.

Star 5 Minimum M_{CO} and M_C							
ε	$M_{CO,min}$ $(M_\odot)$	$M_{C,min}$ $(M_\odot)$	a (AU)	a_{CO} (AU)	a_C (AU)	RL_{CO} (AU)	RL_C (AU)
0.0	21 ± 10	21 ± 9	2.4 ± 0.3	1.2 ± 0.3	1.2 ± 0.4	1.32 ± 0.16	1.1 ± 0.3
0.25	19 ± 10	19 ± 8	2.4 ± 0.3	1.2 ± 0.3	1.2 ± 0.4	1.28 ± 0.15	1.1 ± 0.3
0.5	13 ± 7	13 ± 6	2.1 ± 0.2	1.1 ± 0.3	1.1 ± 0.4	1.14 ± 0.13	1.0 ± 0.3
0.75	6 ± 3	6 ± 3	1.60 ± 0.18	0.8 ± 0.2	0.8 ± 0.3	0.9 ± 0.1	0.7 ± 0.2
0.9	1.7 ± 0.9	1.7 ± 0.7	1.06 ± 0.12	0.5 ± 0.2	0.5 ± 0.2	0.58 ± 0.07	0.48 ± 0.14

Table 2.2: Minimum masses of the compact object (M_{CO}) and the different values of eccentricity, assuming an inclination companion star (M_C) for five angle of 90° [Gottlieb, 2021]. (*RL* - Roche Lobe radius).

We will be obtaining spectra of XID 6592, XID 13, and Star 5 using MOS with FLAMINGOS-2 to further monitor the presence of the Brγ emission line and variability of equivalent widths of the CO bands. In addition to this, we will be getting spectra of new potential XRBs.

As mentioned earlier, due to the high density of compact objects and stellar objects in the GC, it is inevitable that there will be a high rate of tidal captures, which could explain the amount of BH-XRBs and NS-XRBs [Generozov et al., 2018]. The small number of high mass stars in the GC and their shorter lifetimes indicate that the number of HMXBs would be low. However, tidal capture rate of stars that orbit along the plane of the disk of

the galaxy and in the same direction (disk stars) are increased by larger stars, larger escape speeds, and higher stellar densities [Generozov et al., 2018].

This implies that there should be a population of XRBs with main sequence donor stars towards the GC, but RG or RSG donor stars have been found.

Chandra has detected significant X-ray emission with a size of $\sim$ 1" and a luminosity of $\sim 10^{33}$ ergs s^{-1}. This signal was suggested to be produced by several thousand late-type main sequence stars that hide within the central $\sim$ 0.1 parsec towards the GC. Due to tidal spin-ups with other stars and other stellar remnants, these late-type main sequence stars should be rapidly rotating and have a hot coronae, emitting X-rays with temperatures kT a few keV [Sazonov et al., 2012].

CHAPTER 3: METHODOLOGY

Materials and Software

I utilized Python, Gemini MOS Mask Preparation Software (GMMPS), Astronomical Data Query Language (ADQL), superFATBOY (sFB) pipeline, and previously obtained spectra from LUCI/LBT. This spectra was observed on April 21st, 2011, and was left without reduction. Using Gemini Observatory's mask making software, GMMPS, I designed 3 MOS slit masks for FLAMINGOS-2 centered on XID 6592, XID 13, and Star 5 including XRB candidates that I will be further classifying. GMMPS is ran in PyRAF, a command language for Image Reduction and Analysis Facility (IRAF) based on Python.

I used ADQL to retrieve the LUCI spectra in the LBT archives, and used Python to organize and retrieve headers for information. After my data was prepped, I processed them through the sFB pipeline. Due to sFB not previously being compatible with the LUCI instrument, much troubleshooting was encountered. In order for the telluric star spectra to be properly divided with our object spectra, we must write a Python script extension for sFB. This extension will be done in the future. Using Python, I was able to calculate the accretion velocities by obtaining the full width at half maximum (FWHM) of those spectra with Brγ emission lines.

GMMPS and Slit Mask Preparation

Our observation dates were scheduled the nights of July 7th and July 8th, 2023. We designed our slit masks, sent them to Gemini North for cutting, and had them shipped to Gemini South in time for pre-observation set up. When designing in GMMPS, we took the approach of using target lists and 'pseudo-images'.

The first step in designing the three masks started with acquiring our target list with the following columns of data for our XRB candidates: ID, RA, Dec, and magnitude. This data was acquired from the Infrared Side Port Imager (ISPI) instrument as part of the Víctor M. Blanco 4-meter Telescope. Then, a corresponding visual image with WCS keywords was obtained from previous near-infrared Visible and Infrared Survey Telescope for Astronomy (VISTA) data. Our three masks were centered on XID 6592, XID 13, and Star 5, individually, in order to follow up on the characteristics of them. This was additionally a safety margin if our other candidates did not align, we still at least have spectra of the center XRB. I turned our images into pseudo-images by activating the Gemini IRAF conda environment and running PyRAF. This made the image look as if it were taken with Gemini South in order to be easily interpreted by GMMPS and FLAMINGOS-2. Within PyRAF I ran the task `gmskcreate`, which is located in `gemini.gmos.mostools`. I ran `gmskcreate` with all of the following parameters defined below for all three slit masks individually.

XID13 gmskcreate Parameters	
indata="f2_13*mask*1.*cat*"|	Input ASCII table with proper header
inimage="f2_13*mask*.*fits*"|	Input image .fits with WCS
gprgid="GS-2023A-Q-141"|	Our Gemini program ID
instrume="flamingos2"|	Instrument we are using
rafield="266.259360"|	RA value of field center
decfield="-28.963730"|	Dec value of field center
pa="65"|	Position angle
iraunits="degrees"|	Units in the input catalog
fraunits="degrees"|	Units for our rafield value

Table 3.1: Parameters used to produce the XID13 mask using GMMPS.

XID6592 gmskcreate Parameters	
indata="f2_6592mask1.cat"|	Input ASCII table with proper header
inimage="f2_6592mask.fits"|	Input image .fits with WCS
gprgid="GS-2023A-Q-141"|	Our Gemini program ID
instrume="flamingos2"|	Instrument we are using
rafield="266.369970"|	RA value of field center
decfield="-29.161880"|	Dec value of field center
pa="95"|	Position angle
iraunits="degrees"|	Units in the input catalog
fraunits="degrees"|	Units for our rafield value

Table 3.2: Parameters used to produce the XID6592 mask using GMMPS.

Garner 5 `gmskcreate` Parameters	
`indata="f2_garnermask1.cat"|`	Input ASCII table with proper header
`inimage="f2_garnermask.fits"|`	Input image .fits with WCS
`gprgid="GS-2023A-Q-141"|`	Our Gemini program ID
`instrume="flamingos2"|`	Instrument we are using
`rafield="266.425720"|`	RA value of field center
`decfield="-28.957432"|`	Dec value of field center
`pa="72"|`	Position angle
`iraunits="degrees"|`	Units in the input catalog
`fraunits="degrees"|`	Units for our rafield value

Table 3.3: Parameters used to produce the Garner 5 mask using GMMPS.

After successfully running `gmskcreate`, it gave an output of our pseudo-image and a reformatted target list to be interpreted by GMMPS, called an Object Table (OT). After this was done properly, I inputted these two corresponding files into GMMPS. After opening both files, we can start designing our mask and telling GMMPS to ignore sources that would overlap while maintaining 3 acquisition stars within the mask. This stage required me to run `gmskcreate` multiple times with different position angles to see what position angle would maximize the amount of high priority objects within our mask. Below are the three slit masks complete.

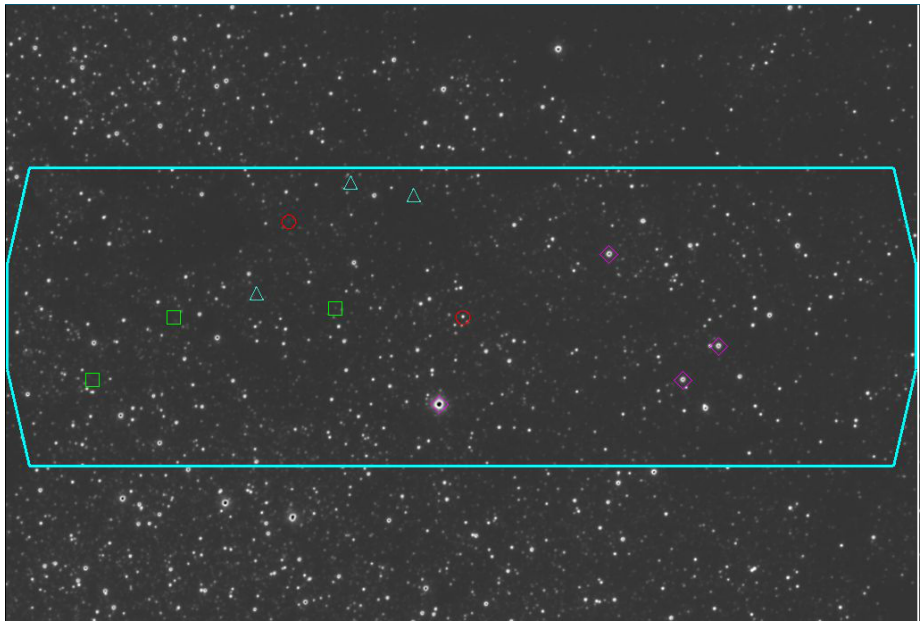

Figure 3.1: FLAMINGOS-2 slit mask of XID 13-centered field, designed using GMMPS. Red circles, green squares, blue triangles, and purple diamonds are 1st priority, 2nd priority, 3rd priority, and acquisition stars, respectively.

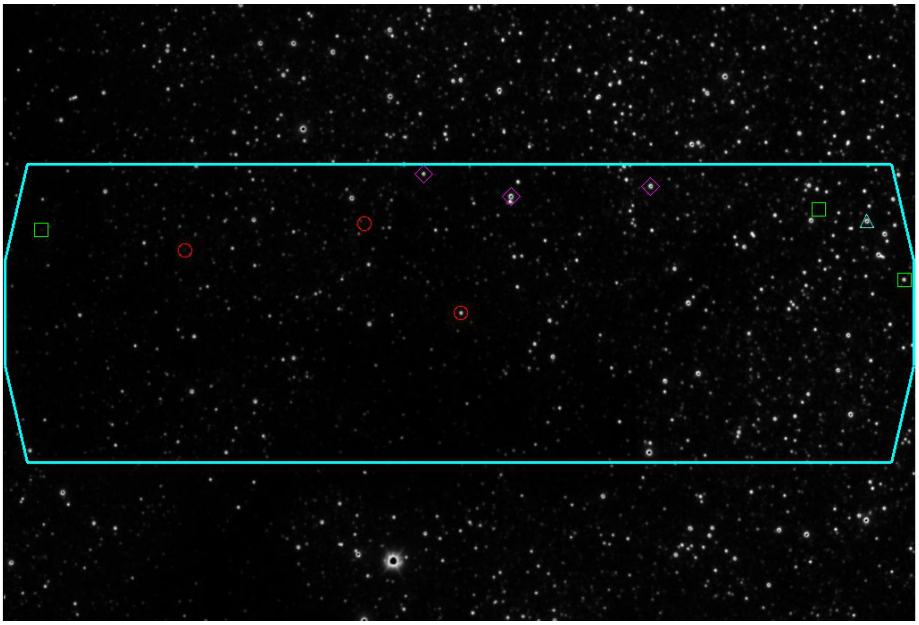

Figure 3.2: FLAMINGOS-2 slit mask of XID 6592-centered field, designed using GMMPS.

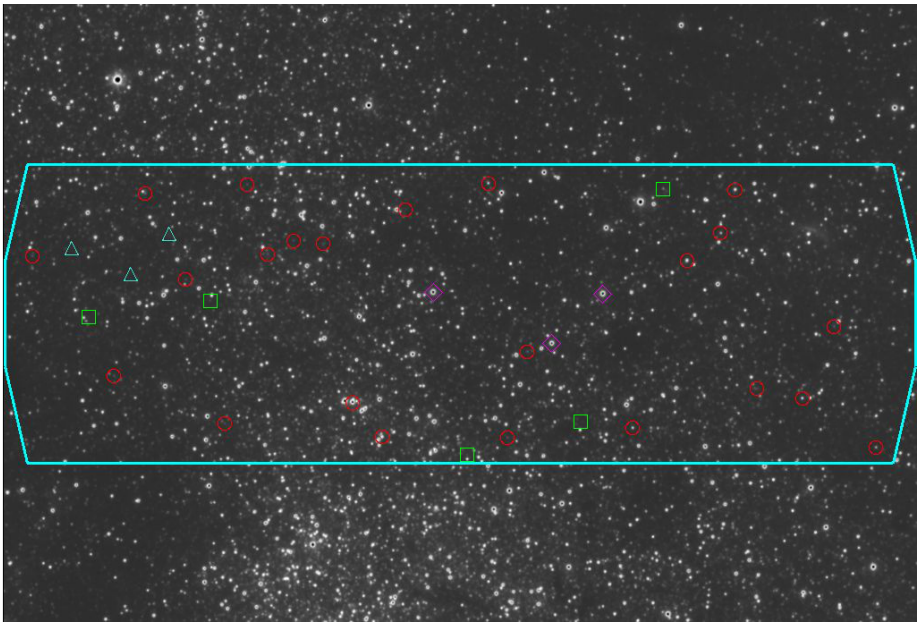

Figure 3.3: FLAMINGOS-2 slit mask of Garner 5-centered field, designed using GMMPS.

The nights of July 7th and July 8th, 2023 in Cerro Pachón had poor sky conditions and we were unable to get any data. However, we are scheduled for future observations in May, June, and July of 2024. This future data will be added in a future revision.

LUCI sFB Data Reduction

While awaiting our future Gemini South observations, we pivoted to previously observed LUCI spectra. This spectra was observed on April 21st, 2011, and was left without reduction. We also have data from other runs, i.e. June 4th, 2011, June 6th, 2011, and June 9th, 2012. For this thesis, we solely reduced the April 21st, 2011 data using sFB, an

XML-controlled GPU-enabled Python pipeline. The data from this observation date can be located in Table A.1.

To preface, sFB has not been previously used for the LUCI/LBT instrument, and has only been used for the Optical System for Imaging and low-Intermediate-Resolution Integrated Spectroscopy (OSIRIS) and MIRADAS as part of the Gran Telescopio Canarias. Thus, there was much troubleshooting and developments along the data reduction process.

Using ADQL, we successfully acquired the A1689 telluric standard spectra, acquisition, objects, arc lamps, spectroscopic flat fields, and dark fields from the LBT archives. Firstly, to use sFB, we must curate a working XML file to inform what parameters sFB should run with. Particularly, our LUCI data was done with MOS with a horizontal dispersion. Due to sFB not having a LUCI extension, we opted to use the general datatype script, `datatype = "spectrum"`. Within our XML file, we determined for sFB to perform the following processes: `noisemap`, `darkSubtract`, `createCleanSkies`, `createMasterArclamps`, `findSlitlets`, `cosmicRaysSpec`, `flatDivideSpec`, `badPixelMaskSpec`, `skySubtractSpec`, `rectify`, `doubleSubtract`, `shiftAdd`, `wavelengthCalibrate`, and `extractSpectra`.

Our first sFB error flagged that all files lacked a native `OBSTYPE = 'OBJECT'` header value. To fix this, we manually added this header value. The next problem was during the `findSlitlets` process, where it attempted to auto-detect slitlets by tracing each slitliet individually. This would not work very well or at all due to some of the slits nearly overlapping with each other. We can get past this by providing an already exisitng region file or making a region file by hand by visually looking at the spectra in SAOImageDS9.

We opted to make the region file by hand and made a separate XML file describing the location of each slitlet and their widths and heights in pixels. We then had sFB use this as our region file. Below, are the 24 traced slitlets.

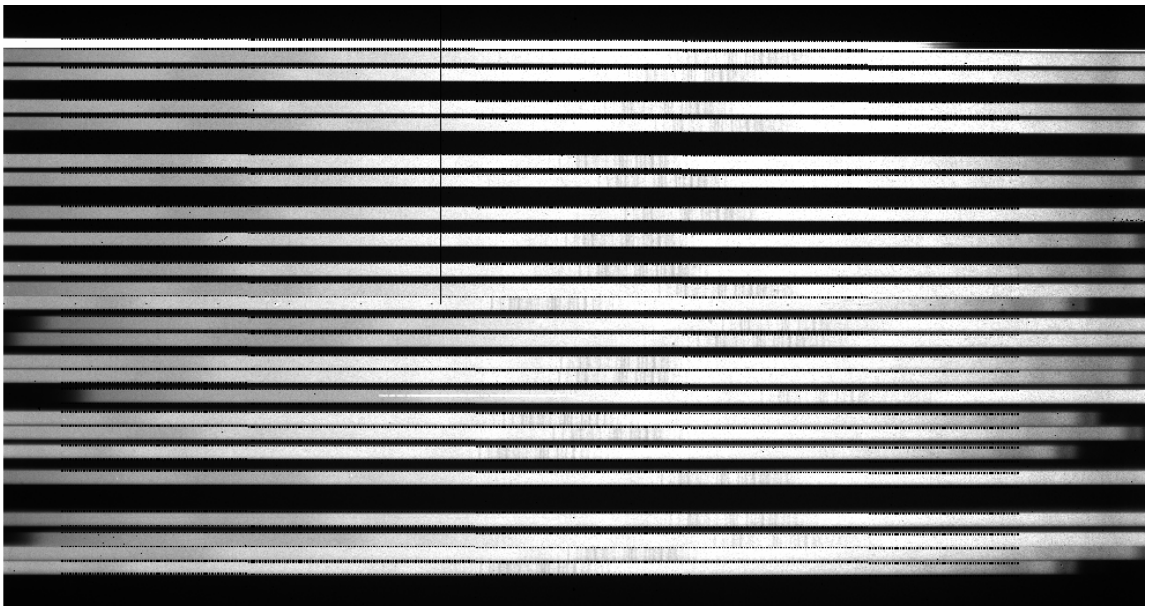

Figure 3.4: Traced slitlets of LUCI MOS spectra.

After this, we found it necessary to do `doubleSubtract` since the residuals were quite bad after the spectra was rectified. The next hurdle was during the `wavelengthCalibrate` process. To start the process, you must provide a wavelength scale guess to get it started. Since the wavelength is being read right to left for LUCI, a negative wavelength scale guess was necessary. After having a good guess, we had to then deduce the optimal option for fitting our spectral lines. We had the option of using OH emission lines or using our arc lamps. For LUCI, the arc lamps are Ne, Ar, and Xe. Attempting different fits, the

OH lines provided the better fit. Having a good wavelength scale guess and fit, our sigma for the residuals of each slitlet was ~ 0.1px. From this, sFB calculated the wavelength solution for each slit, so we know how many microns there are per pixel. After this, the spectra was extracted in a resampled form, where the data was resampled to a linear scale using the standard CD matrix keywords in the FITS header. This resampling fixes the x-axis and shifts them to their appropriate wavelengths. The extracted resampled spectra was then plotted using Python and further analyzed for any characteristic emission or absorption lines. The only part left of reduction is the calibrated star division. This step in the reduction requires a Python script extension to be written to help sFB finish the rest for LUCI data. This will be finished and future revisions will be done.

CHAPTER 4: FINDINGS

From our 24 slits, 3 did not extract, 6 have CO absorption lines, and Slit 19 has strong Brγ emission lines, strong HeII emission line, and small CO absorption lines. With such strong Brγ emission lines, accretion due to a compact object is extremely likely. Slit 19 also has a strong HeII emission line and small CO absorption lines, indicating a possible red giant donor star.

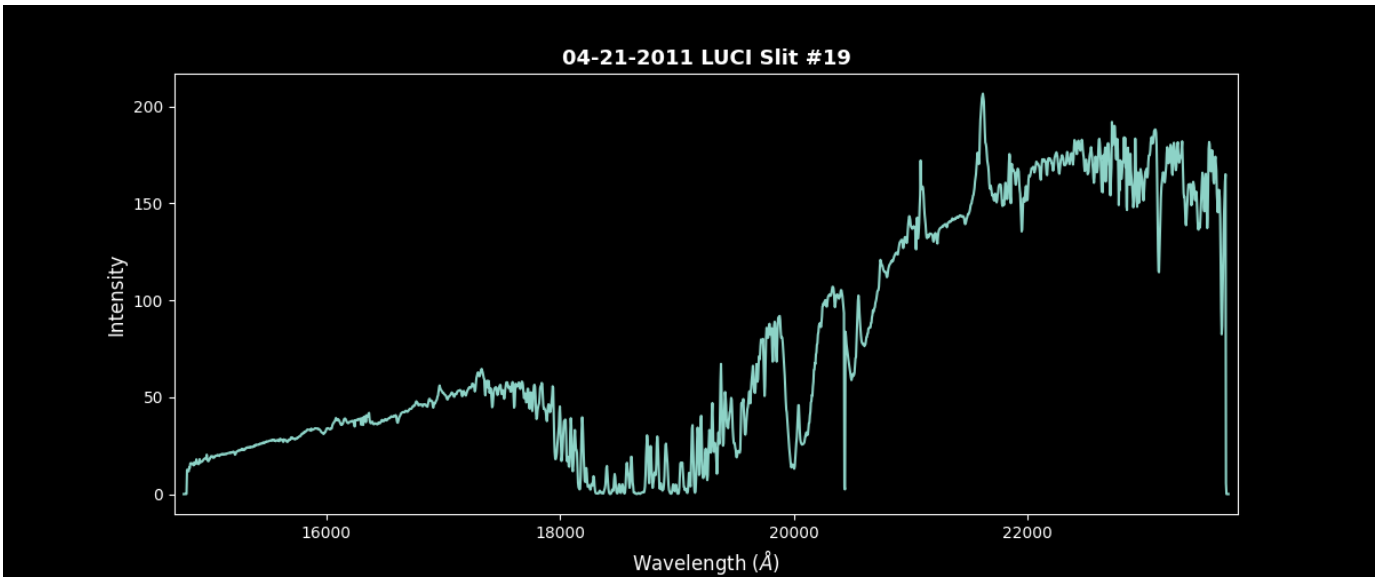

Figure 4.1: Slit 19 extracted spectra, without calibrated star division. Strong Brγ and HeII emission lines, as well as small CO absorption lines are present. This likely indicates that a compact object is present, with a potential red giant.

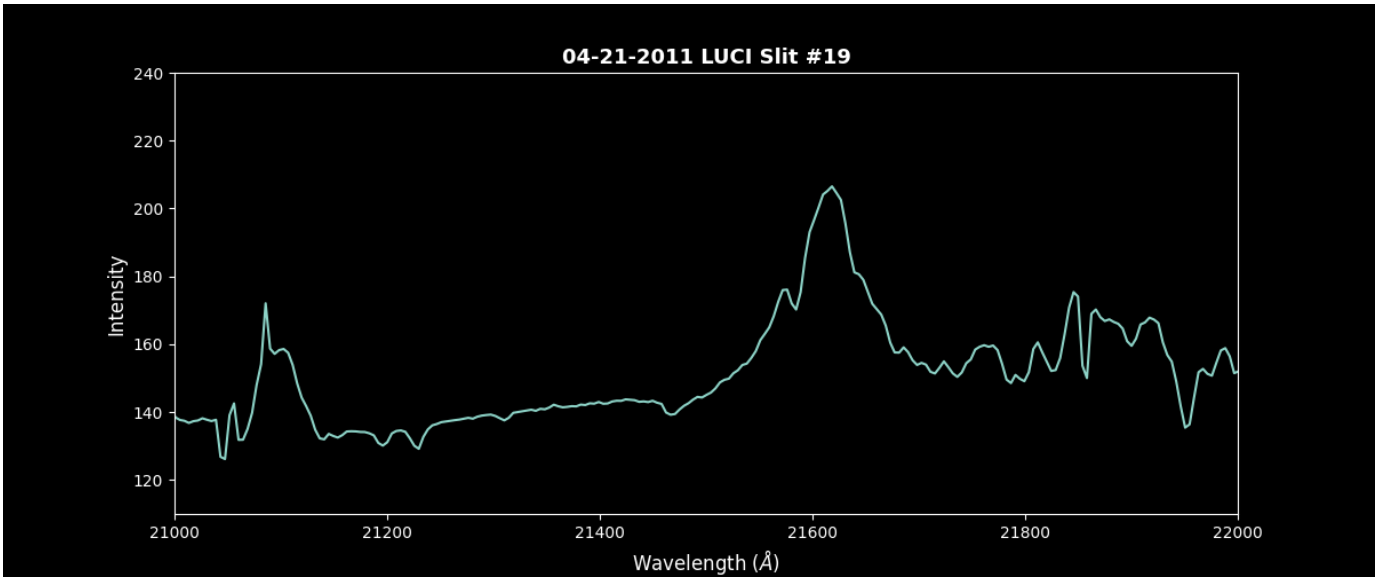

Figure 4.2: Slit 19 extracted spectra, without calibrated star division. Zoomed into the Brγ emission line.

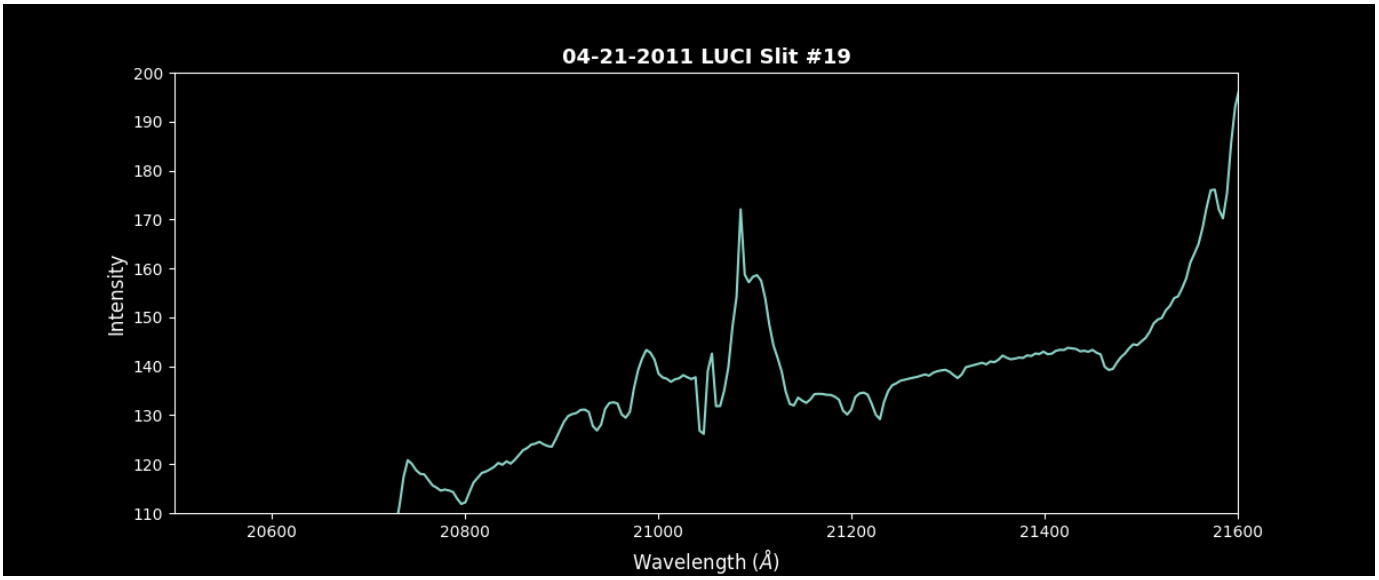

Figure 4.3: Slit 19 extracted spectra, without calibrated star division. Zoomed into the HeII emission line.

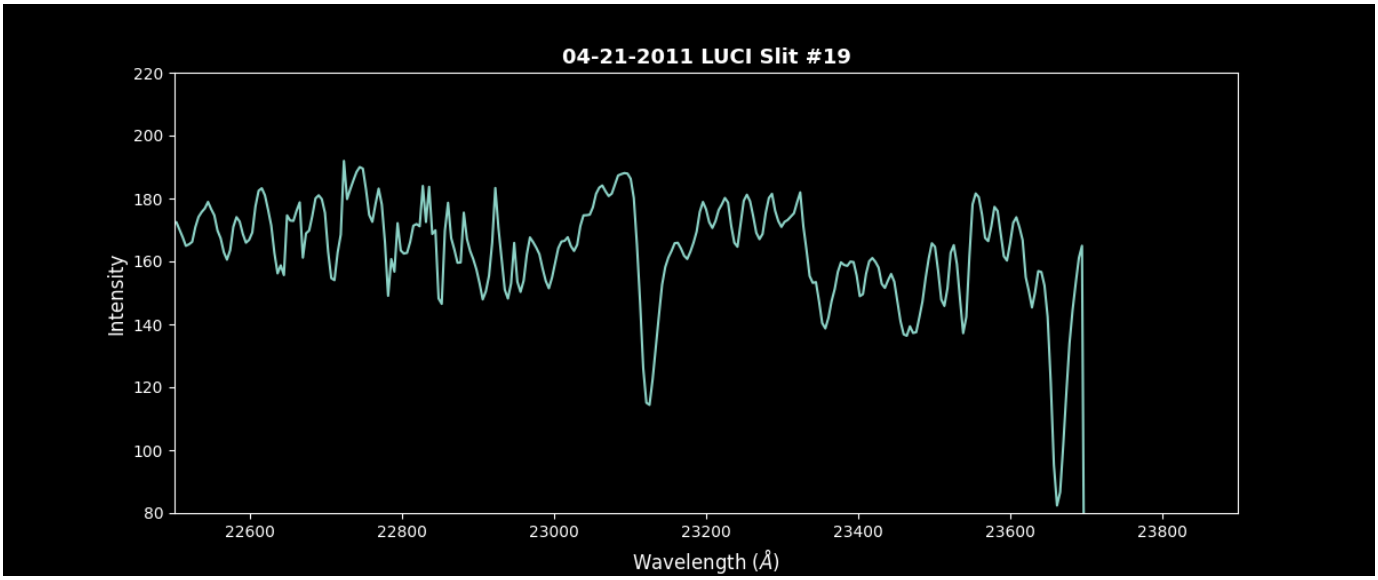

Figure 4.4: Slit 19 extracted spectra, without calibration star division. Zoomed into the CO absorption lines.

By using Python, I calculated the FWHM for the two peaks of the Brγ emission lines to be $\Delta\lambda_1 = 46$ for the smaller peak, and $\Delta\lambda_2 = 60$ for the larger peak. By using the following equations,

$$v_1 = \frac{\Delta\lambda_1}{\lambda_{rest1}}\, c \tag{4.1}$$

$$v_2 = \frac{\Delta\lambda_2}{\Delta\lambda_{rest2}}\, c \tag{4.2}$$

I determined $v_1 = 637\ km/s$ and $v_2 = 829.2\ km/s$. This is incredibly fast, and certainly illustrates the presence of a compact object.

CHAPTER 5: CONCLUSION

Out of the 24 slits of the LUCI/LBT data observed on April 21st, 2011, Slit 19 very likely has a compact object with a possible red giant donor star illustrated by its strong Brγ and HeII emission lines and small CO absorption lines. Its accretion velocities were estimated to be $v_1 = 637\ km/s$ and $v_2 = 829.2\ km/s$. Once the calibrated star division is done, we will have even cleaner spectra, which may reveal other interesting emission or absorption lines in the other spectra. In addition, we have 3 more observation dates of LUCI spectra to reduce and prospective Gemini South spectra that will be observed in May, June, and July of 2024. Many additions to this thesis are to be made in the future.

APPENDIX : LUCI DATA

Table A.1: LUCI observation data from 4/21/2011. Data retrieved from the LBT archives using ADQL.

LUCI 4/21/2011			
File Name	RA	Dec	Type
luci.20110421.0119.fits	+11:16:11.905048924	-03:28:15.078141358	A1689 Telluric
luci.20110421.0120.fits	+11:16:15.816767221	-03:28:37.412860962	A1689 Telluric
luci.20110421.0121.fits	+11:16:15.816767122	-03:28:37.912930712	A1689 Telluric
luci.20110421.0122.fits	+11:16:15.816766347	-03:28:38.212914474	A1689 Telluric
luci.20110421.0123.fits	+11:16:15.816765228	-03:28:38.212797105	A1689 Telluric
luci.20110421.0124.fits	+11:16:16.083958726	-03:28:38.212653232	A1689 Telluric
luci.20110421.0125.fits	+11:16:15.816764979	-03:28:38.212695652	A1689 Telluric
luci.20110421.0157.fits	+17:45:42.080922858	-28:57:23.334802228	Acquisition
luci.20110421.0158.fits	+17:45:42.080922858	-28:57:23.334802228	Acquisition
luci.20110421.0159.fits	+17:45:42.080928662	-28:57:23.334855700	Acquisition
luci.20110421.0160.fits	+17:45:42.426319758	-28:57:25.450492391	Acquisition
luci.20110421.0161.fits	+17:45:41.826546612	-28:57:23.600311807	Acquisition
luci.20110421.0162.fits	+17:45:41.929985807	-28:57:24.240025613	Object
luci.20110421.0163.fits	+17:45:41.929726681	-28:57:24.212900475	Object
luci.20110421.0164.fits	+17:45:41.723127089	-28:57:22.960829811	Object
luci.20110421.0165.fits	+17:45:41.723131298	-28:57:22.960870748	Object
luci.20110421.0166.fits	+17:45:41.723135424	-28:57:22.960911638	Object
luci.20110421.0167.fits	+17:45:41.723164117	-28:57:22.959307596	Object

Continuation of Table A.1			
File Name	RA	Dec	Type
luci.20110421.0168.fits	+17:45:41.930006893	-28:57:24.240195600	Object
luci.20110421.0169.fits	+17:45:41.930010074	-28:57:24.240216953	Object
luci.20110421.0170.fits	+17:45:41.930013281	-28:57:24.240242878	Object
luci.20110421.0171.fits	+17:45:41.930016410	-28:57:24.240254881	Object
luci.20110421.0172.fits	+17:45:41.723159938	-28:57:22.961153561	Object
luci.20110421.0173.fits	+17:45:41.723163691	-28:57:22.961180982	Object
luci.20110421.0174.fits	+17:45:41.723167496	-28:57:22.961219110	Object
luci.20110421.0175.fits	+17:45:41.723171199	-28:57:22.961251223	Object
luci.20110421.0176.fits	+17:45:41.930078035	-28:57:24.240329210	Object
luci.20110421.0177.fits	+17:45:41.930035409	-28:57:24.240335133	Object
luci.20110421.0178.fits	+17:45:41.930038440	-28:57:24.240346137	Object
luci.20110421.0179.fits	+17:45:41.930041437	-28:57:24.240350829	Object
luci.20110421.0180.fits	+17:45:41.723189643	-28:57:22.961367337	Object
luci.20110421.0181.fits	+17:45:41.723193166	-28:57:22.961390634	Object
luci.20110421.0182.fits	+17:45:41.723196647	-28:57:22.961406943	Object
luci.20110421.0183.fits	+17:45:41.723200019	-28:57:22.961418235	Object
luci.20110421.0184.fits	+17:45:41.930057143	-28:57:24.240363300	Object
luci.20110421.0185.fits	+17:45:41.930060177	-28:57:24.240358691	Object
luci.20110421.0186.fits	+17:45:41.930065894	-28:57:24.240350340	Arc Lamp Off
luci.20110421.0187.fits	+17:45:41.930677090	-28:57:24.170499258	Arc Lamp On
luci.20110421.0188.fits	+17:45:41.930067920	-28:57:24.240338374	Arc Lamp Off

Continuation of Table A.1			
File Name	RA	Dec	Type
luci.20110421.0189.fits	+17:45:41.930068874	-28:57:24.240335375	Arc Lamp On
luci.20110421.0190.fits	+17:45:41.930070336	-28:57:24.240339890	Spec Flat Off
luci.20110421.0191.fits	+17:45:41.930070585	-28:57:24.240338174	Spec Flat Off
luci.20110421.0192.fits	+17:45:41.930070876	-28:57:24.240336803	Spec Flat Off
luci.20110421.0193.fits	+17:45:41.930071238	-28:57:24.240325449	Spec Flat Off
luci.20110421.0194.fits	+17:45:41.930071399	-28:57:24.240337867	Spec Flat Off
luci.20110421.0195.fits	+17:45:41.930071925	-28:57:24.240324499	Spec Flat On
luci.20110421.0196.fits	+17:45:41.930072086	-28:57:24.240334162	Spec Flat On
luci.20110421.0197.fits	+17:45:41.930072471	-28:57:24.240321177	Spec Flat On
luci.20110421.0198.fits	+17:45:41.929492786	-28:57:24.293023053	Spec Flat On
luci.20110421.0199.fits	+17:45:41.930073024	-28:57:24.240315329	Spec Flat On
luci.20110421.0238.fits	+17:30:03.934737203	+15:00:10.897893282	Dark Field
luci.20110421.0239.fits	+17:30:03.934737203	+15:00:10.897893282	Dark Field
luci.20110421.0240.fits	+17:30:03.934737203	+15:00:10.897893282	Dark Field
luci.20110421.0241.fits	+17:30:03.934740488	+15:00:10.897990745	Dark Field
luci.20110421.0242.fits	+17:30:03.934740488	+15:00:10.897990745	Dark Field
luci.20110421.0243.fits	+17:30:03.934740488	+15:00:10.897990745	Dark Field
luci.20110421.0244.fits	+17:30:03.934743765	+15:00:10.898087774	Dark Field
luci.20110421.0245.fits	+17:30:03.934743765	+15:00:10.898087774	Dark Field
luci.20110421.0246.fits	+17:30:03.934743765	+15:00:10.898087774	Dark Field
luci.20110421.0247.fits	+17:30:03.934747310	+15:00:10.898182359	Dark Field

Continuation of Table A.1			
File Name	RA	Dec	Type
luci.20110421.0248.fits	+17:30:03.934747310	+15:00:10.898182359	Dark Field
luci.20110421.0249.fits	+17:30:03.934747310	+15:00:10.898182359	Dark Field
luci.20110421.0250.fits	+17:30:03.934750854	+15:00:10.898274486	Dark Field
luci.20110421.0251.fits	+17:30:03.934750854	+15:00:10.898274486	Dark Field
luci.20110421.0252.fits	+17:30:03.934750854	+15:00:10.898274486	Dark Field

LIST OF REFERENCES

A. Avakyan, M. Neumann, A. Zainab, V. Doroshenko, J. Wilms, and A. Santangelo. Xrbcats: Galactic low-mass x-ray binary catalogue. *Astronomy Astrophysics*, 675:A199, 2023. doi: 10.1051/0004-6361/202346522. URL `http://astro.uni-tuebingen.de/~xrbcat/`.

L. A. Balona and D. Ozuyar. Tess observations of be stars: a new interpretation. *Monthly Notices of the Royal Astronomical Society*, 493:25282544, 2020. doi: 10.1093/mnras/staa389.

E. Bozzo, P. Romano, C. Ferrigno, and L. Oskinova. The symbiotic x-ray binaries sct x-1, 4u 1700+24 and igr j17329-2731. *Monthly Notices of the Royal Astronomical Society*, 513:42–54, 2022. doi: 10.1093/mnras/stac907.

Curtis DeWitt, Reba M. Bandyopadhyay, Stephen S. Eikenberry, Kris Sellgren, Robert Blum, Knut Olsen, Franz E. Bauer, and Ata Sarajedini. Three new galactic center x-ray sources identified with near-infrared spectroscopy. *The Astronomical Journal*, 146:109, 2013. doi: 10.1088/0004-6256/146/5/109.

Curtis Noel DeWitt. *Infrared Studies of Galactic Center x-Ray Sources.* PhD thesis, University of Florida, 2011.

V. Doroshenko, S. N. Zhang, A. Santangelo, and et al. Hot disc of the swift j0243. 6+6124 revealed by insight-hxmt. *Monthly Notices of the Royal Astronomical Society*, 491:1857–1867, 2020. doi: 10.1093/mnras/stz2879.

Francis Fortin, Federico García, Adolfo Simaz Bunzel, and Sylvain Chaty. A catalogue of high-mass x-ray binaries in the galaxy: from the integral to the gaia era. *Astronomy Astrophysics*, 671:A149, 2023. doi: 10.1051/0004-6361/202245236.

Alan Garner. *Probing the Galactic Center with CIRCE.* PhD thesis, University of Florida, 2018.

A. Generozov, N. C. Stone, B. D. Metzger, and J. P. Ostriker. An overabundance of black hole x-ray binaries in the galactic centre from tidal captures. *Monthly Notices of the Royal Astronomical Society*, no. 3:4030–4051, 2018. doi: 10.1093/mnras/sty1262.

Amy Gottlieb. *Infrared Studies of X-ray Binaries in the Galactic Center.* PhD thesis, University of Florida, 2021.

Amy M. Gottlieb, Stephen S. Eikenberry, Kendall Ackley, Curtis DeWitt, and Amparo Marco. Rapidly varying red supergiant x-ray binary in the galactic center. *The Astrophysical Journal*, no. 1:32, 2020. doi: 10.3847/1538-4357/ab90ff.

GRAVITY Collaboration, Abuter, R., Aimar, N., Amaro Seoane, P., Amorim, A., Bauböck, M., Berger, J. P., Bonnet, H., Bourdarot, G., Brandner, W., Cardoso, V., Clénet, Y., Davies, R., de Zeeuw, P. T., Dexter, J., Drescher, A., Eckart, A., Eisenhauer, F., Feuchtgruber, H., Finger, G., Förster Schreiber, N. M., Foschi, A., Garcia, P., Gao, F., Gelles, Z., Gendron, E., Genzel, R., Gillessen, S., Hartl, M., Haubois, X., Haussmann, F., HeiSSel, G., Henning, T., Hippler, S., Horrobin, M., Jochum, L., Jocou, L., Kaufer, A., Kervella, P., Lacour, S., Lapeyrère, V., Le Bouquin, J.-B., Léna, P., Lutz, D., Mang, F., More, N., Ott, T., Paumard, T., Perraut, K., Perrin, G., Pfuhl, O.,

Rabien, S., Ribeiro, D. C., Sadun Bordoni, M., Scheithauer, S., Shangguan, J., Shimizu, T., Stadler, J., Straub, O., Straubmeier, C., Sturm, E., Tacconi, L. J., Vincent, F., von Fellenberg, S., Widmann, F., Wielgus, M., Wieprecht, E., Wiezorrek, E., and Woillez, J. Polarimetry and astrometry of nir flares as event horizon scale, dynamical probes for the mass of sgr a*. *AA*, 677:L10, 2023. doi: 10.1051/0004-6361/202347416. URL https://doi.org/10.1051/0004-6361/202347416.

Charles J. Hailey, Kaya Mori, Franz E. Bauer, Michael E. Berkowitz, Jaesub Hong, and Benjamin J. Hord. A density cusp of quiescent x-ray binaries in the central parsec of the galaxy. *Nature*, no. 7699:70–73, 2018. doi: 10.1038/nature25029.

Rolf-Peter Kudritzki and Joachim Puls. Winds from hot stars. *Annual Review of Astronomy and Astrophysics*, 38:613–666, 2000. doi: 10.1146/annurev.astro.38.1.613.

R. Launhardt, R. Zylka, and P. G. Mezger. The nuclear bulge of the galaxy. *Astronomy Astrophysics*, 384:112–139, 2002. doi: 10.1051/0004-6361:20020017.

J. C. Mauerhan, A. Cotera, H. Dong, M. R. Morris, Q. D. Wang, S. R. Stolovy, and C. Lang. Isolated wolfrayet stars and o supergiants in the galactic center region identified via paschen- excess. *The Astrophysical Journal*, 725(1):188, nov 2010. doi: 10.1088/0004-637X/725/1/188. URL https://dx.doi.org/10.1088/0004-637X/725/1/188.

Kumiko Morihana, Masahiro Tsujimoto, Ken Ebisawa, and Poshak Gandhi. Deep near-infrared imaging observation of the faint x-ray point sources constituting the galactic bulge x-ray emission. *Publications of the Astronomical Society of Japan*, 74:283297, 2022. doi: 10.1093/pasj/psab124.

M. P. Muno, F. E. Bauer, F. K. Baganoff, R. M. Bandyopadhyay, G. C. Bower, W. N. Brandt, and et al. A catalog of x-ray point sources from two megaseconds of chandra observations of the galactic center. *The Astrophysical Journal Supplement Series*, 181: 110–128, 2009. doi: 10.1088/0067-0049/181/1/110.

Marvin Neumann, Artur Avakyan, Victor Doroshenko, and Andrea Santangelo. Xrbcats: Galactic high mass x-ray binary catalogue. 2023. doi: 10.48550/arXiv.2303.16137. URL `http://astro.uni-tuebingen.de/~xrbcat/`.

Kerstin Perez, Charles J. Hailey, Franz E. Bauer, Roman A. Krivonos, Kaya Mori, Frederick K. Baganoff, Nicolas M. Barrière, Steven E. Boggs, Finn Erland Christensen, and William W. Craig. Extended hard-x-ray emission in the inner few parsecs of the galaxy. *Nature*, 520:646–649, 2015. doi: 10.1038/nature14353.

S. Sazonov, R. Sunyaev, and M. Revnivtsev. Coronal radiation of a cusp of spun-up stars and the x-ray luminosity of sgr a*. *Monthly Notices of the Royal Astronomical Society*, 420:388–404, 2012. doi: 10.1111/j.1365-2966.2011.20043.x.

Thomas M. Tauris and Edward P. J. van den Heuvel. Formation and evolution of compact stellar x-ray sources. *Cambridge Astrophysics Series*, no. 39:623–665, 2006. doi: 10.2277/0521826594.

Zhenlin Zhu, Zhiyuan Li, and Mark R. Morris. An ultradeep chandra catalog of x-ray point sources in the galactic center star cluster. *The Astrophysical Journal Supplement Series*, 235:26, 2018. doi: 10.3847/1538-4365/aab14f.